Effects of hydration on the structure and compressibility of wadsleyite, β-(Mg₂SiO₄)

Christopher M. Holl,[1,*] Joseph R. Smyth,[1] Steven D. Jacobsen,[2] and Daniel J. Frost[3]

[1]Department of Geological Sciences, University of Colorado, Boulder, Colorado 80309, U.S.A.
[2]Department of Earth and Planetary Sciences, Northwestern University, Evanston, Illinois 60208, U.S.A.
[3]Bayerisches Geoinstitut, Universität Bayreuth, Bayreuth 95440, Germany

Abstract

A suite of pure magnesian wadsleyite (β-Mg₂SiO₄) samples containing 0.005, 0.38, 1.18, and 1.66 wt% H₂O was studied by single-crystal X-ray diffraction to determine the effects of hydration on cation ordering and crystal symmetry. Separate compressibility experiments were carried out to 9.6 GPa to determine the effects of hydration on isothermal equations of state. Crystal-structure refinements at ambient conditions show cation vacancies order onto the M3 site. The most hydrous sample (1.6 wt% H₂O) displayed monoclinic symmetry with $\beta = 90.090(7)°$, whereas the samples with lower content were statistically orthorhombic. The density of wadsleyite decreases with increasing water content at STP according to the empirical relation, $\rho = 3.470(2) - 0.046(2) \, C_{H_2O}$ g/cm³ (with C_{H_2O} in wt% H₂O). Bulk moduli and pressure derivatives of wadsleyite are $K_{T0} = 173(5)$ GPa, $K'_0 = 4.1(15)$ for 0.005 wt% H₂O; $K_{T0} = 161(4)$ GPa, $K'_0 = 5.4(11)$ for 0.38 wt% H₂O; $K_{T0} = 158(4)$ GPa, $K'_0 = 4.2(9)$ for 1.18 wt% H₂O; and $K_{T0} = 154(4)$ GPa, $K'_0 = 4.9(11)$ for 1.66 wt% H₂O. Variation of the bulk modulus of wadsleyite with water content is non-linear, which may be attributable to softening of the structure by ordering of vacancies onto two non-equivalent M3 sites (M3a and M3b) and an accompanying dilution of orthorhombic symmetry.

Keywords: Wadsleyite, bulk modulus, equation of state, nominally anhydrous minerals, mantle Transition Zone

Introduction

Wadsleyite (β-Mg₂SiO₄) is the stable polymorph of olivine in the mantle Transition Zone from 410 to 525 km depth. The olivine-wadsleyite (α-β) transition of Mg₂SiO₄ is thought to produce the seismic discontinuity at 410 km (e.g., Ringwood 1975; Jeanloz and Thompson 1983; Bina and Wood 1987). Wadsleyite is a sorosilicate, isostructural with spinelloid III in the Ni-aluminosilicate system (Moore and Smith 1970; Akaogi and Navrotsky 1984). Because of the presence of an underbonded oxygen site (O1) not bonded to Si, Smyth (1987) predicted that wadsleyite could incorporate significant amounts of water as hydroxyl. Further theoretical studies based on crystal-chemical models (Smyth 1994) predicted that up to 3.3 wt% H₂O could be accommodated by fully protonating the non-silicate oxygen. The presence of variable amounts of hydroxyl in laboratory-synthesized wadsleyite samples was confirmed by Raman and infrared spectroscopy (McMillan et al. 1991; Young et al. 1993).

Inoue et al. (1995) synthesized hydrous wadsleyite at 15.5 GPa and 1200 °C containing 3.1 wt% H₂O (determined by secondary ion mass spectrometry, SIMS), close to the theoretical limit of 3.3 wt% H₂O. The water storage capacity of wadsleyite coexisting with hydrous melt decreases above ~1300 °C, but re-

mains as high as ~1 wt% H₂O at 1400 °C and 15 GPa (Demouchy et al. 2005). Because of the unusually high water storage capacity of β-Mg₂SiO₄, knowledge of the elastic properties of hydrous wadsleyite is needed to constrain the potential hydration state of the mantle Transition Zone from geophysical observation (e.g., van der Lee and Wiens 2006).

The incorporation of water as hydroxyl into wadsleyite and other nominally anhydrous minerals (NAMs) generally requires divalent cation vacancies, which can strongly influence physical properties such as elasticity (e.g., Jacobsen 2006) and rheology (e.g., Karato 2006). Water affects melting and phase relations (e.g., Inoue 1994; Hirschmann 2006; Komabayashi 2006), the depth and pressure interval of phase transitions (e.g., Wood 1995; Smyth and Frost 2002; Chen et al. 2002; Frost and Dolejš 2007), electrical conductivity (e.g., Karato 1990; Huang et al. 2005), strain rates and viscosity (e.g., Hirth and Kohlstedt 1996; Mei and Kohlstedt 2000), and shear strength (e.g., Jung and Karato 2001; Kavner 2003).

Because the mass of liquid-water equivalent that may be stored or recycled through the solid mantle could amount to several oceans, the incorporation of water into mantle minerals has implications for understanding the crust-mantle evolution and regulation of ocean levels (Drake and Righter 2002; Bercovici and Karato 2003). Hydrogen has an indefinite atomic radius resulting in geochemical properties that are strongly pressure and temperature dependent. Smyth et al. (2006) and Mosenfelder et al. (2006) showed that the solubility of OH in olivine increases with

* Present address: Department of Earth and Planetary Sciences, Northwestern University, Evanston, Illinois 60208, U.S.A. E-mail: chrish@earth.northwestern.edu

pressure and temperature, reaching a maximum of about one weight percent H_2O at 12 GPa and 1250 °C, suggesting that hydrogen is more geochemically compatible at conditions near the 410 km discontinuity. Therefore, H may be exchanged between the upper mantle and Transition Zone without severe limitations imposed by dehydration melting, maintaining a deep water cycle between the Transition Zone and the surface (e.g., Smyth and Jacobsen 2006). Hydrogen is probably the least well-constrained compositional variable in current geochemical models of the mantle.

Published compressibility studies of hydrous wadsleyite are limited to one composition with 2.5 wt% H_2O (SIMS) using powder X-ray diffraction to 8.5 GPa (Yusa and Inoue 1997), who reported an isothermal bulk modulus (K_{T0}) as 155(2) GPa, with pressure derivative (K') fixed at 4.3; significantly lower than $K_{T0} = 170–173$ GPa, determined in studies of anhydrous wadsleyite by Zha et al. (1997), Li et al. (1998), Hazen et al. (2000), and the current study. Smyth et al. (1997) described a hydrous (2.3 wt% H_2O) iron-bearing (Fo_{95}) wadsleyite with monoclinic $I2/m$ symmetry, but did not report its equation of state. Smyth et al. (1997) attributed the dilution of symmetry from orthorhombic to monoclinic in hydrous Fe-bearing wadsleyite as resulting from possible ordering of cations and vacancies within two non-equivalent M3 sites. Kudoh and Inoue (1999) reported monoclinic pure-Mg wadsleyite with 2.5 wt% H_2O and suggested that monoclinic symmetry resulted from stacking arrangement of Mg-vacant structural modules. The data of Jacobsen et al. (2005) show a trend of increasing β-angle with water content up to 90.125(3)° at 1.06 wt% H_2O, however, Kohn et al. (2002) report orthorhombic symmetry in iron-free wadsleyite with ~1.5 wt% H_2O.

We have undertaken a systematic study of iron-free hydrous wadsleyites with varying water contents to determine the effects of incorporated hydrogen on their structures and elastic properties. Samples in this study were synthesized at 14 GPa and 1300 °C using starting materials with consistent cation ratios so that the only major compositional variable was H. Variation in observed properties can therefore be reasonably attributed to differences in water content alone. Unit-cell parameters from well-characterized single-crystal samples were collected to precisely determined volumes of hydration and to identify deviation from orthorhombic symmetry. Crystal structure refinements were performed to observe systematic changes in the structure with water content and determine the degree of vacancy ordering. Single-crystal static compression experiments were performed to determine axial and bulk compression, and to relate trends in these values to the observed structural changes. The ultimate goal is to develop a systematic understanding of the relationships between composition, structure, and elastic properties of hydrous wadsleyite, which can be applied to interpreting seismic observations of the Earth's mantle.

EXPERIMENTAL METHODS

Synthesis

All three hydrous samples in this study were synthesized using the 1200 ton Sumitomo multi-anvil press at Bayerisches Geoinstitut, Universität Bayreuth, Germany. Starting materials consisted of mixtures of forsterite (Mg_2SiO_4), and brucite ($MgOH_2$), with additional MgO and SiO_2 added in proportions to produce a slight silica excess and the desired water concentrations. Final water contents for the three starting material batches (unadjusted for silica excess) were 5.0, 2.5, and

1.2 wt%. Starting materials were sealed in welded 2 mm diameter Pt capsules, and loaded in 18 mm sintered-MgO octahedra with a stepped $LaCrO_3$ heaters. The press used 32 mm WC cubes with 8 mm corner truncations. Synthesis conditions were 14 GPa and 1300 °C to simulate upper Transition Zone conditions; pressure was maintained for 20 h with a nominal 12 h heating cycle. Starting water concentrations and results of synthesis runs are presented in Table 1. Sample SS0401 contained roughly equal quantities of wadsleyite and clinoenstatite + quenched melt; samples SS0402 and SS0403 contained traces (>5%) of clinoenstatite and quenched melt, with melt concentrated at the capsule ends. Water contents in wadsleyite were determined using the b/a axial ratio calibration of Jacobsen et al. (2005). The water content for SS0403 was verified by polarized FTIR spectroscopy using the calibration of Libowitzky and Rossman (1997) and found to be in excellent agreement. The other two samples produced total absorption of IR radiation at the principal O-H stretching frequencies for wadsleyite, therefore only minimum water contents could be determined by FTIR absorption for these samples. Because there is no absolute calibration for water in wadsleyite, uncertainties in water content were estimated at 10% for plotting and fitting purposes. For comparative and normalization purposes, we also performed structure refinements of a nominally anhydrous sample (WS3056) from the study of Jacobsen et al. (2005).

Ambient condition XRD

Peak-position centering was carried out using a Siemens/Bruker P4 diffractometer with a dual scintillation point detector and an 18 kW rotating Mo anode source with single-crystal graphite monochromator. Calibration using a ruby standard was performed for each analysis to adjust for small shifts in the effective $MoK\alpha_1$-$K\alpha_2$ mixed wavelength induced by the monochromator geometry. For unit-cell parameter determination, eight equivalent positions of at least 12 unique reflections were centered and the cell constants determined from linear and non-linear least squares refinements of the centered peak positions. Unit-cell parameters are listed in Table 2.

Intensity data were collected on a Bruker P4 diffractometer equipped with a Bruker APEX II CCD area detector with v. 2.0 controller software on the same 18 kW generator. Phi and omega scans were performed at set 2θ intervals, covering all of reciprocal space to at least 75° in 2θ with at least fourfold redundancy for the hydrous samples, and to 55° in 2θ for the nearly anhydrous sample WS3056. Resolution for WS3056 was limited due to the small size of the crystal. An automated absorption correction routine was performed by the APEX II control software during data reduction. Refinements were performed using the program SHELXL-97 (Sheldrick 1997) available in the WinGX software package (Farrugia 1999). Scattering factors used in the refinements for Mg^{2+}, Si^{4+}, and O^{1-} were from Cromer and Mann (1968), and those for O^{2-} were from Tokonami (1965). Various modeling schemes for oxygen were used, with oxygen modeled as entirely O^{2-} ions or as various mixtures of O^{2-} and O^{1-}. Hydrogen positions were not modeled in the final refinements, as previous attempts produced high degrees of ambiguity in H positional coordinates and displacement parameters, and adversely affected precision of nearby oxygen positions. Instead, H positions were inferred from systematic structural variation between samples with various water contents. Intensity data collection parameters and structure refinement statistics are listed in Table 2.

High-pressure XRD

Lattice parameters of the hydrous wadsleyite samples were determined at pressures up to ~10 GPa by single-crystal X-ray diffraction in a diamond anvil cell using at least eight unique reflections and their symmetry equivalents in both positive and negative 2θ positions. A modified Merrill-Bassett type diamond anvil cell (Hazen and Finger 1977) with 500 μm culets and hardened steel seats giving a 60° optical aperture was used. The 2θ range was approximately ±10–30° for both ruby and wadsleyite centered peaks. Crystals were oriented and polished parallel to (111) to allow well-distributed observations in reciprocal space, and to minimize differences in axial compression due to non-hydrostatic conditions. A methanol-

TABLE 1. Starting material water concentrations, resulting phases, and resulting wadsleyite water contents for the three synthesis runs

	Starting wt% H_2O	Observed phases	Wadsleyite wt% H_2O
SS0401	5.0	~50% wadsleyite (to 150 μm), ~50% clinoenstatite + melt	1.66
SS0402	2.5	>95% wadsleyite (to 300 μm), <5% clinoenstatite + melt	1.18
SS0403	1.2	>95% wadsleyite (to 400 μm), <5% clinoenstatite + melt	0.38

TABLE 2. Unit-cell symmetry, ambient condition unit-cell parameters, and data collection parameters for wadsleyite

Sample	SS0401	SS0402	SS0403	WS3056
wt% H_2O	1.66	1.18	0.38	0.005
Space group	*I2/m*	*Imma* or *I2/m*	*Imma*	*Imma*
a (Å)	5.6807 (3)	5.6862 (4)	5.6951 (3)	5.7008 (5)
b (Å)	11.5243 (6)	11.5023 (13)	11.4628 (7)	11.4407 (12)
c (Å)	8.2515 (6)	8.2526 (6)	8.2565 (9)	8.2582 (7)
β (°)	90.090 (7)	90.013 (9)	90.001 (9)	90.000 (9)
V (Å³)	540.20 (5)	539.75 (6)	538.99 (6)	538.61 (7)
Maximum 2θ scanned	80°	75°	80°	55°
No. of reflections	4295	3603	5046	2236
No. unique	790	745	1039	354
No. unique with *I* > 4σ	639	604	886	295
R_{int}	0.0288	0.0272	0.0346	0.0403
R_f for *I* > 4σ	0.0271	0.0353	0.0298	0.0268
R_f for all data	0.0352	0.0424	0.0366	0.0359
GoF for all data	0.979	1.324	1.351	1.261

ethanol-water mixture (16:3:1) was used as the pressure medium. Pressure in the cell was determined using the equation of state of quartz (Angel et al. 1997). Ambient condition analysis was performed to check crystal quality and to determine starting unit-cell parameters. The least hydrous samples (WS3056, SS0403) displayed orthorhombic (*Imma*) symmetry, whereas the most hydrous (SS0401) displayed monoclinic symmetry (*I2/m*) with β-angles ranging from 90.09(1) to 90.16(1)°. The crystal with β = 90.09(1)° possessed low mosaicity and produced the lowest cell parameter uncertainties, and therefore was selected for high-pressure study in the DAC. Sample SS0402 displayed variable symmetry among different crystals, although deviation from orthorhombic symmetry was only slightly greater than the uncertainty in the measurement.

RESULTS AND DISCUSSION

Lattice parameters

Room-pressure unit-cell parameters were measured both outside of the DAC for comparison to previous studies (Table 2) and inside the DAC before the addition of the pressure-transmitting medium for equation of state fitting. Parameters were refined in the monoclinic cell (*I2/m*) for SS0401 and in the orthorhombic cell *Imma* for samples SS0402, SS0403, and WS3056. Cell volumes vs. water content from the current study and from Jacobsen et al. (2005) are plotted together in Figure 1a. A linear regression to the current data set gives

$$V = 538.62(5) + 0.95(5) \times C_{H_2O} \text{ Å}^3$$

where C_{H_2O} is the water content in wt% H_2O determined from *b/a* axial ratios (Jacobsen et al. 2005). The volume increase of 0.17% per wt% H_2O in wadsleyite is similar to that in olivine, reported as 0.18% per wt% H_2O (Smyth et al. 2006). For an idealized structure with exactly one-quarter of M3 sites vacant and 3.3 wt% H_2O, $V = 541.76$ Å³ and ρ = 3310 kg/m³. In comparison to thermal expansion, hydrating wadsleyite to 1 wt% H_2O has approximately the same effect on volume as a temperature increase of 550 °C, using the thermal expansion coefficient determined by Inoue et al. (2004). However, the variation of volume with water content in the current study is offset from values determined by Jacobsen et al. (2005). Figure 1a illustrates the problem of comparing absolute volumes measured using different instruments and experimental procedures. A preferable method compares lattice parameters normalized to anhydrous values (Fig. 1b), which allows us to combine the current sample suite with those from Jacobsen et al. (2005) into a merged data
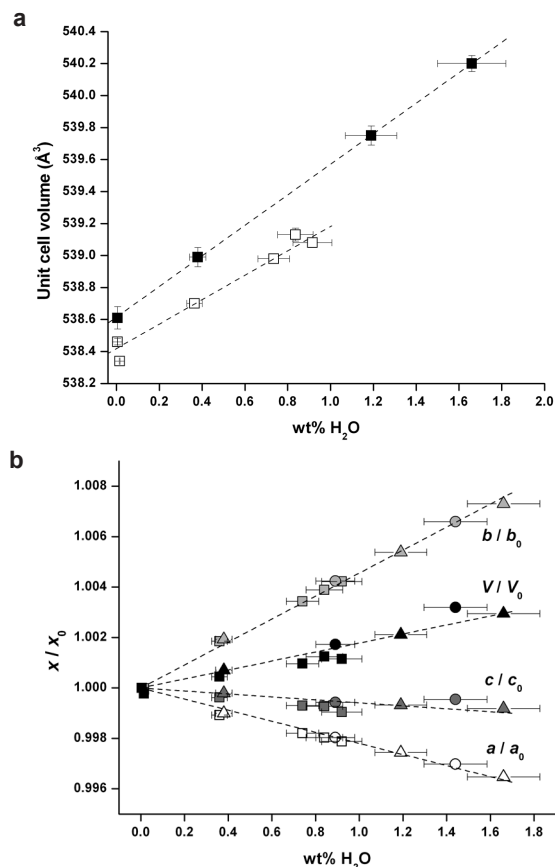
FIGURE 1. Unit-cell volumes vs. water content for Fo₁₀₀ hydrous wadsleyite (**a**). Solid symbols represent the current study, open symbols are data from Jacobsen et al. (2005). Estimated 10% uncertainty in water contents is shown. The data from Jacobsen et al. (2005) were collected on different instruments than in the current study, so direct comparison of absolute volumes is not warranted. Alternatively, all data were normalized against the near-anhydrous value for each set and plotted in **b** to directly compare the relative volumetric and axial expansions. Triangles = SS0401, SS0402, and SS0403 from current study; squares = data from Jacobsen et al. (2005); circles = samples BT1 and BT4 from Kohn et al. (2002).

set. Variation of density with water content was calculated for the entire suite of samples in this manner, resulting in a best-fit to the merged data (Fig. 2):

$$ρ = 3.470(2) - 0.046(2) \, C_{H_2O} \text{ g/cm}^3$$

where C_{H_2O} is water content in wt% H_2O.

Smyth et al. (1997) observed monoclinic symmetry with β angles up to 90.397(9)° in iron-bearing (Fo₉₄) hydrous wadsleyite with 2.25 wt% H_2O. Violation of orthorhombic symmetry was attributed to ordering of H and Mg onto non-equivalent M3 sites normally related by a mirror plane perpendicular to the **a**-axis in the nominal structure. Vacancies in the M3 sites are introduced by substitution of H (which is thought to reside along the O-O edges and not in the M sites themselves) and trivalent (Fe^{3+}) cations for Mg (in the case of Fe-bearing wadsleyite). In iron-
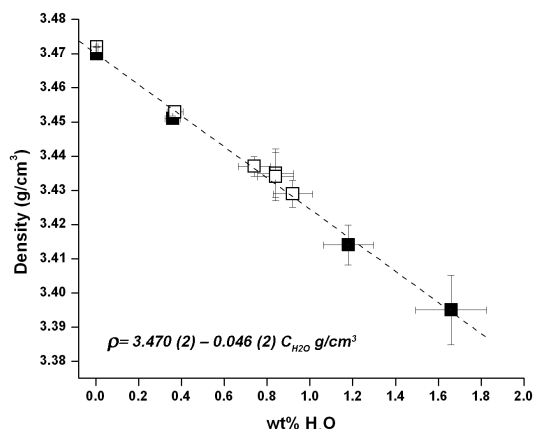
FIGURE 2. Density vs. water content for Fo_{100} hydrous wadsleyite. Solid symbols represent the current study, open symbols are data from Jacobsen et al. (2005). Estimated 10% uncertainty in water contents is shown. The best-fit line is shown for the merged data sets.

free wadsleyite, monoclinic symmetry was confirmed by Kudoh and Inoue (1999). If monoclinic symmetry is due to vacancy ordering onto two non-equivalent M3 sites upon quenching, the two sites would have differing compressibilities, and increasing pressure would increase the β angle. Therefore, β angles were refined for SS0401 at high pressure in the diamond cell to track changes in the β angle with increasing pressure, however, no systematic variation was observed. Also, as discussed below, the crystals show signs of strain due to polysynthetic twinning on the orthorhombic cell which further limits the precision of β-angle measurement.

Structure refinements

Refined atomic positions, cation site occupancy factors, and displacement parameters are presented in Tables 3 and 4. Selected interatomic distances and polyhedral parameters are presented in Table 5. Refined parameters for WS3056 are in agreement with Hazen et al. (2000) for anhydrous wadsleyite. Constraining occupancy factors to unity (Table 3) did not alter the refinement statistics or position parameters significantly. Refinements with oxygen modeled entirely as O^{2-} resulted in lower R_f values than for those in which oxygen was modeled as a mixture of O^{2-} and O^{1-} ions. These refinements resulted in occupancy factors in better agreement with measured water contents; therefore, results presented here are based on refinements using only O^{2-} scattering factors for oxygen. Additionally, it was assumed that no Si occupied octahedral sites. Using these assumptions, all three samples show full occupancy of the M1 and M2 sites. Nearly all vacancies were ordered onto the M3 site, with vacancy occurring on 13.6%, 11.0%, and 3.9% of available M3 sites for SS0401, SS0402, and SS0403, respectively. The tetrahedral site is fully occupied within statistical uncertainties for all compositions studied. From these results, hydration of wadsleyite appears to be almost entirely accomplished by vacancy on the M3 site, with disorder onto other sites unimportant over this range of water contents. Sample SS0401 was refined in $I2/m$, with the M3 site split into two non-equivalent sites (M3a and M3b) at (¼, 0.123, ¼) and (¾, 0.377, ¼). Occupancy was slightly higher on M3a

TABLE 3. Atomic position coordinates and occupancy factors for wadsleyite

Sample		SS0401	SS0402	SS0403	WS3056
wt% H_2O		1.66	1.18	0.38	0.005
M1	x/a	0	0	0	0
	y/b	0	0	0	0
	z/c	0	0	0	0
M2	x/a	−0.00014(17)	0	0	0
	y/b	¼	¼	¼	¼
	z/c	0.97051(11)	0.97034(11)	0.97005(8)	0.97088(19)
M3	x/a	¼	¼	¼	¼
	y/b	0.12299(9)	0.12426(7)	0.12634(3)	0.12750(8)
	z/c	¼	¼	¼	¼
M3b	x/a	¾			
	y/b	0.37703(10)			
	z/c	¼			
Si	x/a	0.00000(9)	0	0	0
	y/b	0.12083(4)	0.12059(4)	0.12012(2)	0.11990(6)
	z/c	0.61574(5)	0.61601(6)	0.61649(4)	0.61705(10)
O1	x/a	0.0002(3)	0	0	0
	y/b	¼	¼	¼	¼
	z/c	0.2237(2)	0.2214(3)	0.21929(15)	0.2161(4)
O2	x/a	0.0002(3)	0	0	0
	y/b	¼	¼	¼	¼
	z/c	0.7163(2)	0.7160(2)	0.71641(14)	0.7165(4)
O3	x/a	−0.0003(2)	0	0	0
	y/b	0.01245(12)	0.98816(11)	0.98937(6)	0.98993(16)
	z/c	0.74375(14)	0.25591(14)	0.25617(10)	0.2554(3)
O4	x/a	0.2605(2)	0.26118(15)	0.26184(10)	0.2617(3)
	y/b	0.12355(11)	0.12338(8)	0.12297(3)	0.12277(11)
	z/c	0.99419(15)	0.99381(10)	0.99324(7)	0.99216(19)
O4b	x/a	0.7389(2)			
	y/b	0.37644(11)			
	z/c	0.99419(15)			
s.o.f.					
M1 (×¼)		1.0	1.01.0	1.0	
M2 (×¼)		1.0	1.0	1.0	1.0
M3a (×½)		0.871 (2)	0.8900(17)	0.9614(12)	1.0
M3b		0.857(2)			
Si (×½)		1.000 (4)	1.0	1.0	1.0

Notes: SS0401 is reported in the alternate setting space group $I2/m$ with origin shift (¼,¼,¼).

than on M3b, supporting the proposal by Smyth et al. (1997) that the break in orthorhombic symmetry is due to preference for one site of the nonequivalent M3 pair.

Polyhedral edges were examined to identify systematic changes in edge length with water content. The majority of edges displayed lengthening with hydration, consistent with volume expansion of vacant site polyhedra due to the absence of the attracting charge on the site. Four edge lengths were observed to decrease with increasing water content, consistent with the results of Jacobsen et al. (2005). Compared to the anhydrous structure, the shared O4-O4 edges on M1 and M2, and the O1-O1, O1-O4, and O3-O3 edges on M3 decrease systematically by 0.4%, 0.7%, 1.2%, and 0.3% per 1 wt% H_2O, respectively, over the range in water content studied. As noted by Jacobsen et al. (2005), systematic shortening of an octahedral edge with increasing water content suggests a favorable position for H since the positive charge of the H ion mitigates the repulsion between adjacent O ions. However, possible H positions are not limited to the shortened edges, as shown by analyses of FTIR absorption spectra (Jacobsen et al. 2005; Kohn et al. 2002) in which O-H stretching mode absorption peaks are assigned to various other edges in the structure. The current results, however, do appear to indicate a strong preference for protonation along edges associated with O1, supporting the claim by Smyth (1987) that O1 is a preferred site for protonation in the structure due to

TABLE 4. Anisotropic displacement parameters for wadsleyite

Sample		SS0401	SS0402	SS0403	WS3056
M1	U_{11}	0.0137(6)	0.0122(5)	0.0075(3)	0.0050(8)
	U_{22}	0.0069(5)	0.0080(4)	0.00484(20)	0.0024(7)
	U_{33}	0.0165(5)	0.0146(5)	0.0080(3)	0.0086(8)
	U_{23}	0.0028(3)	0.0013(3)	0.00026(16)	−0.0008(5)
	U_{13}	−0.0007(4)	0	0	0
	U_{12}	−0.0005(4)	0	0	0
	U_{eq}	0.0124(3)	0.0116(2)	0.00676(13)	0.0053(4)
M2	U_{11}	0.0085(5)	0.0098(4)	0.0064(3)	0.0057(8)
	U_{22}	0.0047(4)	0.0066(4)	0.00495(14)	0.0020(6)
	U_{33}	0.0076(4)	0.0073(4)	0.0050(2)	0.0073(8)
	U_{23}	0	0	0	0
	U_{13}	0.0000(3)	0	0	0
	U_{12}	0	0	0	0
	U_{eq}	0.0069(2)	0.0079(2)	0.00544(12)	0.0050(4)
M3	U_{11}	0.0067(6)	0.0075(3)	0.0054(2)	0.0045(6)
	U_{22}	0.0106(6)	0.0110(4)	0.00718(19)	0.0043(6)
	U_{33}	0.0078(5)	0.0076(3)	0.0061(2)	0.0073(7)
	U_{23}				
	U_{13}	−0.0005(3)	−0.0007(2)	−0.00084(15)	−0.0012(4)
	U_{12}	0	0	0	0
	U_{eq}	0.0087(4)	0.0087(2)	0.00621(13)	0.0054(4)
M3b	U_{11}	0.0071(6)			
	U_{22}	0.0120(6)			
	U_{33}	0.0086(5)			
	U_{23}	0			
	U_{13}	0.0003(4)			
	U_{12}	0			
	U_{eq}	0.0093(4)			
Si	U_{11}	0.0063(3)	0.0069(2)	0.0043(16)	0.0035(5)
	U_{22}	0.0065(3)	0.0068(2)	0.00411(13)	0.0025(4)
	U_{33}	0.0072(3)	0.0062(2)	0.00377(15)	0.0052(5)
	U_{23}	−0.00023(17)	−0.0001(2)	0.00002(7)	−0.0002(3)
	U_{13}	0.0000(17)	0	0	0
	U_{12}	0.00017(19)	0	0	0
	U_{eq}	0.00666(19)	0.00665(14)	0.00406(9)	0.0037(3)
O1	U_{11}	0.0068(10)	0.0061(8)	0.0047(5)	0.0040(16)
	U_{22}	0.0091(9)	0.0099(7)	0.0052(4)	0.0052(13)
	U_{33}	0.0100(8)	0.0099(8)	0.0065(5)	0.0050(15)
	U_{23}	0	0	0	0
	U_{13}	0.0008(6)	0	0	0
	U_{12}	0	0	0	0
	U_{eq}	0.0086(4)	0.0086(3)	0.00544(19)	0.0048(6)
O2	U_{11}	0.0090(10)	0.0092(9)	0.0070(5)	0.0072(16)
	U_{22}	0.0070(8)	0.0074(7)	0.0035(3)	0.0019(12)
	U_{33}	0.0068(8)	0.0061(7)	0.0037(5)	0.0062(15)
	U_{23}	0	0	0	0
	U_{13}	0.0007(6)	0	0	0
	U_{12}	0	0	0	0
	U_{eq}	0.0076(4)	0.0076(3)	0.00471(19)	0.0051(6)
O3	U_{11}	0.0088(8)	0.0096(7)	0.0065(4)	0.0068(13)
	U_{22}	0.0090(6)	0.0081(5)	0.0048(3)	0.0021(9)
	U_{33}	0.0083(6)	0.0071(6)	0.0049(3)	0.0065(12)
	U_{23}	0.0005(4)	0	0	0
	U_{13}	0.0002(5)	0	0	0
	U_{12}	−0.0003(5)	0	0	0
	U_{eq}	0.0087(3)	0.0083(3)	0.00538(15)	0.0051(5)
O4	U_{11}	0.0075(7)	0.0067(4)	0.0044(3)	0.0048(8)
	U_{22}	0.0056(6)	0.0079(4)	0.0051(2)	0.0027(7)
	U_{33}	0.0085(6)	0.0077(4)	0.0052(2)	0.0077(9)
	U_{23}	0.0006(4)	0.0002(3)	0.00020(15)	−0.0002(5)
	U_{13}	0.0002(4)	0.0011(3)	0.00089(18)	0.0000(5)
	U_{12}	0.0006(5)	0.0003(3)	−0.00016(12)	−0.0004(5)
	U_{eq}	0.0072(3)	0.00744(18)	0.00491(12)	0.0051(4)
O4b	U_{11}	0.0074(7)			
	U_{22}	0.0067(7)			
	U_{33}	0.0080(7)			
	U_{23}	−0.0009(4)			
	U_{13}	−0.0006(4)			
	U_{12}	0.0011(5)			
	U_{eq}	0.0074(3)			

underbonding on the non-silicate oxygen. The M-site polyhedra expand with hydration by 0.5%, 0.3%, and 0.2% per 1 wt% H_2O for M1, M2, and M3, respectively, and the Si tetrahedron expands by 0.2% per 1 wt% H_2O.

Axial compression

Table 6 lists unit-cell parameters for hydrous wadsleyite at pressures up to 9.6 GPa. Linear compressibilities were obtained by calculating linear fits to axial strain vs. pressure. Compressibilities parallel to crystallographic axes (β_a, β_b, β_c) are 0.00147(8), 0.00183(11), and 0.00218(3) GPa^{-1}, respectively, for SS0401; 0.00163(6), 0.00178(3), and 0.00228(3) GPa^{-1} for SS0402; and 0.00163(6), 0.00159(2), and 0.00220(3) GPa^{-1}, respectively for SS0403. Compression is strongly anisotropic with the **c**-axis approximately 40% more compressible than the **a**- and **b**-axes for SS0403 (~0.4 wt% H_2O), consistent with previous compression studies of anhydrous wadsleyite (Hazen et al. 1990, 2000) and predictive models (Kiefer et al. 2001). With the incorporation of axial compression data from Hazen et al. (2000) and Yusa and Inoue (1997) for near-anhydrous and 2.5 wt% H_2O samples, respectively, all axes show increasing compressibility with increasing water content (Fig. 3), although the compressibility increase may be lesser at higher water contents. For the most hydrous sample studied (SS0401, ~1.6 wt% H_2O), the **c**-axis is nearly 50% more compressible than the **a**-axis, but only 20% more compressible than the **b**-axis. A possible explanation of the increase in **b**-axis compressibility is the expansion of the axis with hydration, shown in Figure 1b, due to lengthening of the shared O1-O3 edges of M3 corresponding to the H-bonds. Mitigation of O-O repulsion by these hydrogen bonds may facilitate compression in the preferred overall H-bond direction in the crystal. The **a**- and **c**-axes reach limits to compressibility at lower water concentrations,

Bulk compression

Pressure-volume data were fitted to second and third-order Birch-Murnaghan equations of state using the program EoSFit (Angel 2001). For all fits, V_0 was refined with initial value as the room-pressure volume determined by X-ray diffraction in the DAC before the addition of the pressure medium. Weighting was based on reported uncertainties for both pressure and volume
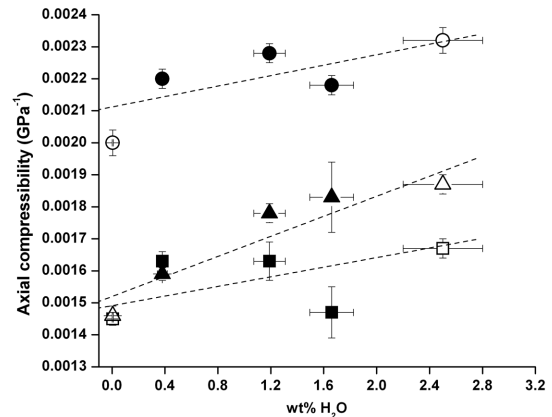
FIGURE 3. Linear compressibility parallel to crystallographic axes for wadsleyite. Squares = **a**-axis; triangles = **b**-axis, circles = **c**-axis. Solid symbols represent the current study; open symbols near 0 wt% are data from Hazen et al. (2000); open symbols at 2.5 wt% are from Yusa and Inoue (1997). Best-fit lines were added to aid in comparing slopes of the data.

TABLE 5. Bond lengths, polyhedral parameters, and polyhedral edge lengths

Sample wt% H_2O		SS0401 1.66	SS0402 1.18	SS0403 0.38	WS3056 0.005	Sample wt% H_2O		SS0401 1.66	SS0402 1.18	SS0403 0.38	WS3056 0.005
M1	M1-O4a ×4	2.0540(13)	2.0548(9)	2.0527(5)	2.0500(13)	Si	Ave. bond	1.6521	1.6514	1.6507	1.6503
	M1-O4b	2.0566(13)					Ave. edge	2.6950	2.6939	2.6927	2.6920
	M1-O3 ×2	2.1193(13)	2.1163(12)	2.1190(8)	2.1123(21)		Ave. angle	109.391	109.39	109.393	109.393
	Ave. bond	2.0766	2.0753	2.0748	2.0708		V	2.303	2.300	2.297	2.294
	Ave. edge	2.9356	2.9337	2.9330	2.9272		TAV	13.715	14.129	14.114	14.972
	Ave. angle	108	108	108	108		TQE	1.004	1.004	1.004	1.004
	V	11.866	11.842	11.831	11.756						
	OAV	13.9952	13.862	14.2918	15.608	Polyhedral edges					
	OQE	1.0044	1.004	1.005	1.005						
						M1	O3-O4a(1)	2.8451	2.8458	2.8503	2.8400
M2	M2-O1	2.090(2)	2.072(2)	2.0583(14)	2.029(4)		O3-O4a(2)	3.0539	3.0501	3.0469	3.0436
	M2-O4a ×4	2.0862(15)	2.0891(9)	2.0930(5)	2.0917(13)		O3-O4b(1)	2.8485			
	M2-O4b	2.0880(15)					O3-O4b(1)	3.0542			
	M2-O2	2.098(2)	2.0988(20)	2.0945(13)	2.101(4)		O4-O4(1)	2.8494	2.8401	2.8214	2.8121
	Ave. bond	2.0893	2.0878	2.0875	2.0828		O4-O4(2)	2.9627	2.9702	2.9824	2.9837
	Ave. edge	2.9483	2.9465	2.9463	2.9411						
	Ave. angle	106.427	106.450	106.472	106.607	M2	O1-O4a	2.8117	2.8024	2.7980	2.7893
	V	12.052	12.027	12.023	11.958		O1-O4b	2.8116			
	OAV	21.401	21.117	20.794	17.6632		O2-O4a	3.0917	3.0955	3.0936	3.0866
	OQE	1.0060	1.006	1.006	1.005		O2-O4b	3.0978			
							O4-O4(1)	2.9627	2.9702	2.9824	2.9837
M3a	M3-O1 ×2	2.0499(15)	2.0417(6)	2.0250(3)	2.0177(8)		O4-O4(2)	2.9143	2.9128	2.9122	2.9112
	M3-O3 ×2	2.1097(15)	2.1152(11)	2.1201(6)	2.1243(16)						
	M3-O4a ×2	2.1117(12)	2.1152(9)	2.1218(6)	2.1310(16)	M3a	O1-O1	2.8703	2.8821	2.8924	2.9033
	Ave. bond	2.0905	2.0907	2.0890	2.0910		O1-O3	3.0364	3.0252	3.0030	2.9933
	Ave. edge	2.9568	2.9570	2.9544	2.9570		O1-O4(1)	2.8117	2.8024	2.7980	2.7893
	Ave. angle	107.016	106.929	106.725	106.594		O1-O4(2)	3.0626	3.0806	3.0977	3.1223
	V	12.096	12.093	12.053	12.072		O3-O3	2.8388	2.8448	2.8494	2.8518
	OAV	16.405	17.829	19.912	23.058		O3-O4(1)	3.0539	3.0501	3.0469	3.0436
	OQE	1.005	1.005	1.006	1.007		O3-O4(2)	2.9215	2.9205	2.9099	2.9161
M3b	M3-O1 ×2	2.0521(16)				M3b	O1-O1	2.8761			
	M3-O3 ×2	2.1118(16)					O1-O3	3.0364			
	M3-O4b ×2	2.1117(12)					O1-O4b(1)	2.8116			
	Ave. bond	2.0919					O1-O4b(2)	3.0652			
	Ave. edge	2.9588					O3-O3	2.8457			
	Ave. angle	107.016					O3-O4b(1)	3.0542			
	V	12.123					O3-O4b(2)	2.9245			
	OAV	16.144									
	OQE	1.005				Si	O2-O3	2.7470	2.7492	2.7532	2.7541
							O2-O4a	2.6449	2.6389	2.6377	2.6331
Si	Si-O4a ×2	1.6369(14)	1.6329(9)	1.6315(6)	1.6310(15)		O2-O4b	2.6411			
	Si-O4b	1.6315(13)					O3-O4a	2.7128	2.7101	2.7075	2.7073
	Si-O3	1.6358(14)	1.6376(13)	1.6374(8)	1.639(2)		O3-O4b	2.7061			
	Si-O2	1.7041(10)	1.7020(10)	1.7021(6)	1.7000(17)		O4a-O4b	2.7180	2.7160	2.7127	2.7171

Note: Angle variance and quadratic elongation for octahedral (OAV, OQE) and tetrahedral (TAV, TQE) sites are measures of the distortion of the internal angles and bond lengths relative to an ideal polyhedron (Robinson et al. 1971).

measurements. Resulting equation of state parameters are given in Table 7, and are illustrated in Figure 4 with comparison to other high-pressure hydrous phases. Bulk modulus decreases with hydration, and all bulk moduli reported are markedly lower than for anhydrous wadsleyite. The trends of bulk modulus with water content and density are not linear, as there is a sharp decrease in bulk modulus between anhydrous wadsleyite and the sample with ~0.4 wt% H_2O, but a more gradual decrease among the hydrous samples. The bulk modulus of ringwoodite (γ-Mg_2SiO_4) was shown to decrease linearly with hydration (Smyth et al. 2004), and bulk moduli of hydrous Mg-silicates (olivine-humite group) vary linearly with density (Ross and Crichton 2001), which as in NAMs is linked to water content. The general trend of hydrous wadsleyite bulk modulus with water content (Fig. 4) was similar to that of grossular-hibschite-katoite (decrease in K of ~4.6 and ~3.7 GPa per 1 wt% H_2O) despite little hydrogarnet-type substitution apparent from the wadsleyite structure refinements. The slope of the wadsleyite trend was less negative than that of ringwoodite but greater than that of the olivine-humite series. Wadsleyite and ringwoodite partially share a $2H^+$ for Mg^{2+} sub-

stitution mechanism, but ringwoodite also undergoes a coupled substitution of $8H^+$ for $2Mg^{2+}$ + Si^{4+} (Kudoh 2001), so the difference in linearity of the corresponding curves may be due to structural differences and kinetic effects during quenching. Yusa and Inoue (1997) report a bulk modulus K_T = 155 (2) GPa and K' fixed at 4.3 for Fo_{100} wadsleyite with ~2.5 wt% H_2O. This value is equivalent to our reported K_T for wadsleyite with only 1.66 wt% H_2O, but an unconstrained fit to their data yields a lower K_T (144 GPa) and a higher K' (7.6). No systematic trend in K' with water content could be determined from the available data, however recent ultrasonic data for hydrous ringwoodite indicate that K' is elevated from about 4 to 5.3 for hydrous ringwoodite containing ~1 wt% H_2O (Jacobsen and Smyth 2006), similar to the current value of K' = 5.4 for wadsleyite with 1.66 wt% H_2O.

This study demonstrates the need for caution when applying data obtained at pressures ≤10 GPa to the Transition Zone. Though high values of K' (>4.0) obtained in this and other studies of OH-bearing nominally anhydrous phases (e.g., Yusa and Inoue 1997; Smyth et al. 2004; Jacobsen and Smyth 2006) accurately model the observed data below 10 GPa, they do not account for

possible effects of K'' at higher pressures. Because it is not always possible to observe the influence of K' in volume-pressure plots, we have plotted all the compression data of hydrous wadsleyite in the current study as Birch normalized pressure F_E (Birch 1978) vs. Euler finite strain f_E (Fig. 5). Jeanloz and Hazen (1991) used this finite strain analysis on compression data sets obtained concurrently from anhydrous wadsleyites with various Fe/Mg ratios. They found that all data sets could be described using a second-order BM EoS and that bulk modulus was independent of composition. From Figure 5, it is apparent that this is not the case form hydrous wadsleyite, and that at least a third-order BM EoS is required to model the current data sets. However, a third-order equation of state with $K' > 4$ results in bulk sound
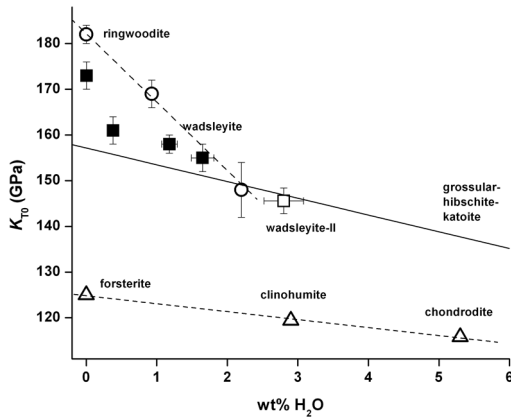
FIGURE 4. Bulk modulus of wadsleyite vs. water content, and comparison with other Mg-silicate series. The dashed line represents the trend of the grossular-hydrogarnet series. Wadsleyite appears to have a non-linear relation of bulk modulus to water content, whereas ringwoodite and the forsterite-hydroxylchondrodite series are shown to have linear relations. References: hydrous wadsleyite = this study; anhydrous wadsleyite = Hazen et al. (2000); ringwoodite = Smyth et al. (2004); forsterite = Downs et al. (1992); OH-clinohumite and OH-chondrodite = Ross and Crichton (2001); grossular-hydrogarnet = Wang and Ji (1997), O'Neill et al. (1993), Lager et al. (2002).
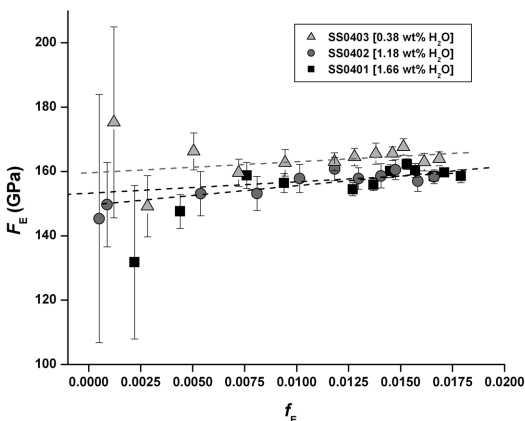

FIGURE 5. Plots of Birch normalized pressure (F_E) vs. Euler finite strain (f_E) for hydrous wadsleyites. Bulk moduli from y-intercepts of linear regressions are 160(3), 153(3), and 149(3) GPa for samples with 0.38, 1.18, and 1.66 wt% H_2O, respectively. Positive slopes of the linear regressions indicate $K' > 4$.

TABLE 6. Unit-cell parameters for hydrous wadsleyite at pressure

P (GPa)	a (Å)	b (Å)	c (Å)	β (°)	V (Å³)
SS0401 (1.66 wt% H_2O)					
0.0001	5.673(2)	11.551(3)	8.251(2)	90.06(2)	540.68(16)
0.87(3)	5.653(3)	11.546(3)	8.229(2)	90.19(2)	537.16(20)
1.99(4)	5.661(3)	11.481(4)	8.210(1)	90.04(2)	533.62(11)
3.74(5)	5.643(2)	11.456(5)	8.177(1)	90.04(2)	528.64(14)
4.62(4)	5.641(2)	11.421(6)	8.161(1)	90.00(2)	525.78(15)
6.85(3)	5.615(2)	11.388(6)	8.119(1)	90.02(2)	519.20(14)
7.46(4)	5.604(2)	11.398(6)	8.110(1)	90.09(3)	518.04(15)
8.18(4)	5.598(3)	11.384(7)	8.098(2)	90.09(3)	516.12(19)
8.56(3)	5.599(2)	11.364(6)	8.091(1)	90.03(2)	514.84(16)
8.90(4)	5.596(1)	11.362(3)	8.087(1)	90.12(2)	514.11(10)
9.32(6)	5.595(3)	11.342(8)	8.082(1)	90.02(2)	512.83(16)
9.58(3)	5.595(3)	11.333(8)	8.076(1)	90.03(2)	512.10(16)
SS0402 (1.18 wt% H_2O)					
0.0001	5.681(2)	11.520(3)	8.249(2)		539.87(16)
0.22(2)	5.678(2)	11.516(2)	8.245(2)		539.06(14)
0.40(2)	5.677(2)	11.508(2)	8.240(2)		538.44(16)
2.54(2)	5.651(2)	11.464(2)	8.201(1)		531.27(14)
5.05(2)	5.635(3)	11.409(4)	8.148(2)		523.85(19)
6.05(3)	5.627(2)	11.394(2)	8.130(2)		521.26(14)
6.55(2)	5.621(2)	11.380(2)	8.122(2)		519.52(17)
7.17(3)	5.612(3)	11.371(3)	8.115(2)		517.88(23)
7.64(2)	5.610(2)	11.366(3)	8.106(2)		516.84(19)
8.06(5)	5.601(2)	11.355(2)	8.100(1)		515.22(15)
8.56(2)	5.602(1)	11.345(2)	8.088(1)		514.05(10)
SS0403 (0.38 wt% H_2O)					
0.0001	5.701(3)	11.464(4)	8.250(2)		539.18(22)
0.64(2)	5.698(3)	11.454(5)	8.231(3)		537.23(32)
2.58(2)	5.676(2)	11.415(4)	8.198(2)		531.12(22)
3.58(2)	5.664(3)	11.393(4)	8.178(2)		527.72(23)
4.83(3)	5.651(3)	11.377(5)	8.154(2)		524.26(22)
6.13(3)	5.641(3)	11.347(4)	8.133(3)		520.60(24)
6.72(3)	5.634(2)	11.344(4)	8.122(2)		519.14(22)
7.34(2)	5.631(4)	11.333(6)	8.111(3)		517.59(34)
7.80(2)	5.627(2)	11.323(4)	8.105(2)		516.38(21)
8.20(3)	5.626(3)	11.316(4)	8.099(3)		515.59(25)
8.54(6)	5.620(2)	11.306(4)	8.091(2)		514.08(22)
9.01(3)	5.619(3)	11.296(4)	8.083(2)		513.01(23)
WS3056 (anhydrous)					
0.0001	5.698 (3)	11.440 (5)	8.257 (2)		538.21 (16)
0.51 (2)	5.694 (2)	11.429 (4)	8.248 (1)		536.76 (16)
1.26 (2)	5.684 (2)	11.415 (3)	8.231 (1)		534.10 (18)
2.30 (3)	5.676 (3)	11.396 (4)	8.214 (1)		531.33 (24)
3.52 (2)	5.669 (2)	11.373 (3)	8.190 (1)		528.03 (15)
5.00 (2)	5.650 (2)	11.352 (3)	8.163 (1)		523.61 (15)
5.57 (3)	5.650 (3)	11.335 (4)	8.155 (1)		522.24 (18)
5.88 (3)	5.644 (2)	11.334 (3)	8.149 (1)		521.33 (15)
6.38 (3)	5.640 (3)	11.321 (5)	8.138 (1)		519.59 (23)
7.00 (3)	5.638 (3)	11.312 (4)	8.130 (1)		518.51 (18)
7.30 (3)	5.633 (2)	11.312 (3)	8.125 (1)		517.73 (13)

velocities that are higher for the hydrous phases than for anhydrous wadsleyite at Transition Zone pressures. The bulk sound velocity of anhydrous wadsleyite and hydrous wadsleyite (0.4 wt% H_2O) are plotted together in Figure 6 using the current third-order Birch-Murnaghan equations of state. For comparison, we also plot the sound velocity of hydrous wadsleyite assuming $K' = 4.0$ (dashed line in Figure 6). To illustrate the importance of K'', we also calculated a hypothetical equation of state (i.e., not fitted to the data) that satisfies two requirements: (1) it is consistent with observed data over the experimental pressure range, and (2) it results in bulk sound velocities that are equal or lower than anhydrous wadsleyite. To satisfy both requirements, hypothetical equation of state parameters $K_0 = 161$ GPa, $K' = 5.1$, and $K'' = -0.1$ GPa^{-1} are required (Fig. 6). Though there is no physical basis for the hypothetical equation of state with $K'' = -0.1$, this exercise is meant only to illustrate what would be

TABLE 7. Equation of state parameters for wadsleyite, presented in order of increasing water content

Reference	wt% H$_2$O	P_{max}(GPa)	V_0 (Å^3)	K_{T0}	K'
Hazen et al. (2000)	0*	10.12	539.26(9)	172(3)	6.3(7)
Zha et al. (1997)	0*	14		170(2)‡	4.3(2)
Li et al. (1998)	0†	7		172(2)‡	4.2(1)
This study, WS3056	0.005	7.30	538.22(12)	173(5)	4.1(15)
			538.21(10)	174(1)	4.0§
This study, SS0403	0.38	9.01	539.23(10)	161(4)	4.9(11)
			539.12(22)	164.7(12)	4.0§
This study, SS0402	1.18	8.56	539.80(10)	158(4)	4.2(9)
			539.75(10)	159.2(8)	4.0§
This study, SS0401	1.66	9.58	540.55(16)	154(4)	5.4(11)
			540.43(14)	160.3(12)	4.0§
Yusa et al. (1997)	2.5	8.5		155(2)	4.3§

Note: Refined zero-pressure volumes are given if they were reported in the referenced study.
* Anhydrous, no Raman hydroxyl peaks observed.
† Assumed anhydrous, no water content given.
‡ Adiabatic bulk modulus.
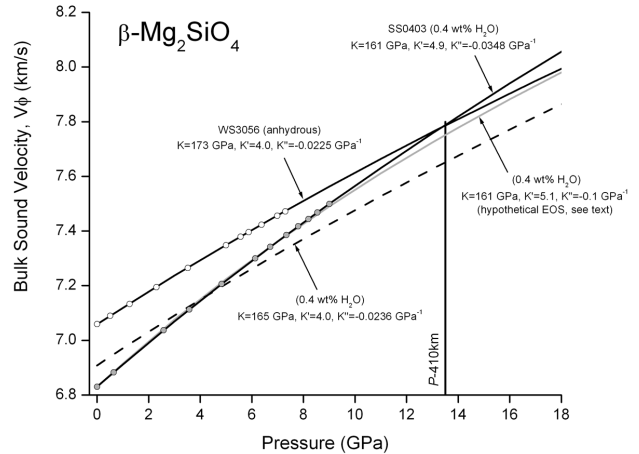§ Fixed value, unrefined during fitting.

FIGURE 6. Bulk sound speed plots for anhydrous and hydrous wadsleyite (solid black curves), and a hypothetical curve representing possible behavior of hydrous wadsleyite at Transition Zone pressures (gray). Curves are extrapolated from zero-pressure Birch-Murnaghan equation of state parameters; data points represent pressures at which volume data were collected. The dashed curve represents a refit of the hydrous data with $K' = 4.0$, consistent with the anhydrous value. The gray curve is calculated from the fitted K_0 and K', with K'' selected so that bulk sound speeds for the hydrous composition remain lower than the speeds for the anhydrous composition through the pressure stability range of wadsleyite in the Transition Zone. The vertical line represents the approximate pressure at the 410 km seismic discontinuity.

Cation ordering

The decrease in bulk modulus with hydration in NAMs is probably due to the large number of M-site cation vacancies required by substitution of OH. These vacancies are initially more compressible than occupied sites, but rapidly stiffen with pressure because of strong O-O repulsive forces in the vicinity of cation vacancy. This is the likely cause of the high K' values seen in static compression studies of NAMs conducted at pressures lower than the stability range of the material in the mantle. In room-temperature compression experiments on wadsleyite, ordering of cations onto a preferred M3 site could result in differing compressibilities for the two M3 sites. The result is that violation of the **a**-normal mirror plane becomes more apparent with pressure, and therefore the deviation from orthorhombic symmetry becomes more pronounced. Behavior under high pressure and high temperature is not known, since high pressure and high temperature tend to have competing effects on cation ordering. (Hazen and Navrotsky 1996)

Monoclinic symmetry in wadsleyite has been observed in various studies for hydrous compositions, but the monoclinic angle and presumably the degree of ordering is variable between samples with similar water contents. In the current study, sample SS0401 was monoclinic with β angle at ambient conditions ranging from 90.09° to 90.16° for a hydrous iron-free composition with ~1.6 wt% H$_2$O. Sample SS0402 (~1.2 wt% H$_2$O) contained some crystals with orthorhombic and some with monoclinic symmetry. All crystals of sample SS0403 (~0.4 wt% H$_2$O) examined were statistically orthorhombic. Smyth et al. (1997) described an iron-bearing wadsleyite with 2.3 wt% H$_2$O and a maximum β-angle of 90.4°. Jacobsen et al. (2005) observed orthorhombic symmetry in samples with 0.32 wt% H$_2$O and below, increasing to β = 90.055(3)° for the sample with 0.6 wt% H$_2$O, and up to 90.125(3)° in the sample with 1.06 wt% H$_2$O. Kohn et al. (2002) report iron-free wadsleyites with orthorhombic symmetry at

needed to satisfy the observed data and keep hydrous velocities below anhydrous velocities at Transition Zone pressures, as well as to emphasize the need for ultrasonic or light scattering measurements of wadsleyite sounds velocities at pressures above 10 GPa.

water contents up to ~1.5 wt%.

If hydrous wadsleyite is orthorhombic at mantle *P-T* conditions, it is likely that differences in quenching rates are partially responsible for the inconsistency in reported β angles. It is unclear if the hydrous samples were monoclinic or orthorhombic at synthesis conditions; however, the presence of strain consistent with fine polysynthetic twinning suggests that they were orthorhombic and that ordering of the vacancies occurred on quench. It may be possible to resolve this question by examination of crystals quenched at different rates.

Sample SS0402 contained wadsleyite crystals with a maximum diameter of ~300 μm. Unit-cell dimensions at ambient conditions were measured for several crystals to characterize symmetry. Roughly half of the crystals were statistically orthorhombic, and half were statistically monoclinic with β angles ranging to approximately 90.1°. To identify possible internal strain, directional scans in reciprocal space were performed on both orthorhombic and monoclinic crystals from SS0402. A representative scan set is shown in Figure 7. Significant relative peak broadening was observed in the **c*** direction of the orthorhombic sample and in the **b*** direction of the monoclinic crystal. Strain in the orthorhombic structure may be related to polysynthetic twinning normal to (0 0 1), whereas strain in the monoclinic structure may be primarily due to distortion of the edge-sharing M3 quartets. Data collection using the CCD area detector revealed no significant peaks inconsistent with either *Imma* or *I*2/*m* indicative of possible polytypism. No relative broadening was observed in the **a*** direction, but possible peak splitting in the monoclinic sample was observed, perhaps related to violation of the mirror plane normal to **a***.
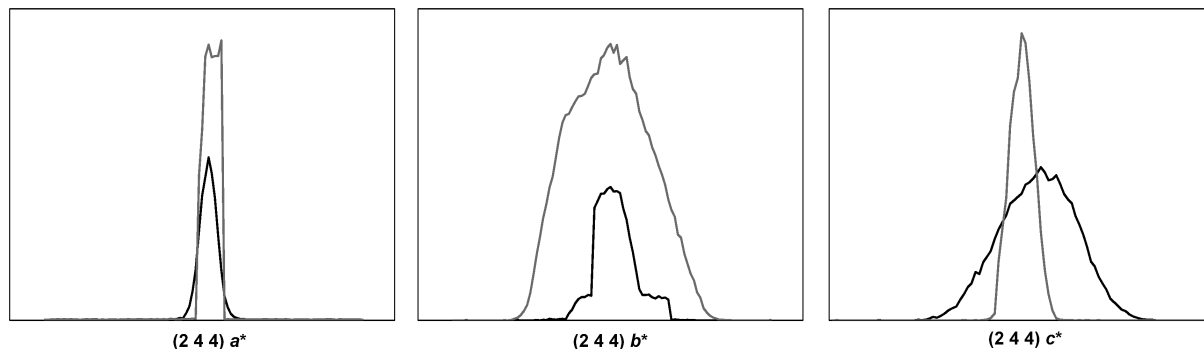
FIGURE 7. Omega scans of the (2 4 4) diffraction peak for two separate wadsleyite crystals from sample SS0402. Black = orthorhombic crystal; gray = monoclinic crystal. Width of scan field is approximately 1.5°. Broadening in the monoclinic sample is interpreted to result from polysynthetic twinning.

ACKNOWLEDGMENTS

REFERENCES CITED

Angel, R.J. (2001) EoSFit, a program for fitting equations of state to *P-V-T* data. Version 5.2. Crystallography Laboratory, Virgina Tech, Blacksburg (http://www.crystal.vt.edu/crystal/software.html).

Angel, R.J., Miletich, R., and Finger, L.W. (1997) The use of quartz as an internal pressure standard in high-pressure crystallography. Journal of Applied Crystallography, 30, 461–466.

Bercovici, D. and Karato, S. (2003) Whole-mantle convection and the transition-zone water filter. Nature, 425, 35–44.

Bina, C.R. and Wood, B.J. (1987) Olivine-spinel transitions: experimental and thermodynamic constraints and implications for the nature of the 400 km seismic discontinuity. Journal of Geophysical Research, 92, 4853–4866.

Chen, J., Inoue, I., Yurimoto, H., and Weidner, D.J. (2002) Effect of water on olivine-wadsleyite phase boundary in the (Mg,Fe)$_2$SiO$_4$ system. Geophysical Research Letters, 29, 1875, DOI: 10.1029/2001GL014429.

Cromer, D.T. and Mann, J. (1968) X-ray scattering factors computed from numerical Hartree-Fock wave functions. Acta Crystallographica, A24, 321–325.

Demouchy, S., Deloule, E., Frost, D.J., and Keppler, H. (2005) Temperature and pressure dependence of water solubility in iron-free wadsleyite. American Mineralogist, 90, 1084–1091.

Downs, R.T., Zha, C-S., Duffy, T.S., and Finger, L.W. (1996) The equation of state of forsterite to 17.2 GPa and the effects of pressure media. American Mineralogist, 81, 51–55.

Drake, M.J. and Righter, K. (2002) Determining the composition of the Earth. Nature, 416, 39–44.

Farrugia, L.J. (1999) WinGX software package. Journal of Applied Crystallography, 32, 837–838.

Frost, D.J. and Dolejš, D. (2007) Experimental determination of the effect of H$_2$O on the 410-km seismic discontinuity. Earth and Planetary Science Letters, 256, 182–195, DOI: 10.1016/j.epsl.2007.01.023.

Hazen, R.M. and Finger, L.W. (1977) Modifications in high-pressure single-crystal diamond-cell techniques. Carnegie Institution of Washington Year Book, 76, 655–656.

Hazen, R.M., Zhang, J., and Ko, J. (1990) Effects of Fe/Mg on the compressibility of synthetic wadsleyite, β-(Mg$_{1-x}$Fe$_x$)$_2$SiO$_4$, (x < 0.25). Physics and Chemistry of Minerals, 17, 416–419.

Hazen, R.M., Weinberger, M.B., Yang, H., and Prewitt, C.T. (2000) Comparative high-pressure crystal chemistry of wadsleyite, β-(Mg$_{1-x}$Fe$_x$)$_2$SiO$_4$, with x = 0 and 0.25. American Mineralogist, 85, 770–777.

Hirschmann, M.M. (2006) Water, melting, and the deep earth H$_2$O cycle. Annual Review of Earth Planetary Sciences, 34, 629–653.

Hirth, G. and Kohlstedt, D.L. (1996) Water in the oceanic upper mantle: Implications for rheology, melt extraction and the evolution of the lithosphere. Earth and Planetary Science Letters, 144, 93–108.

Huang, X., Xu, Y., and Karato, S. (2005) Water content in the Transition Zone from electrical conductivity of wadsleyite and ringwoodite. Nature, 434, 746–749.

Inoue, T. (1994) Effects of water on melting phase relations and melt composition in the system Mg$_2$SiO$_4$-MgSiO$_3$-H$_2$O to 15 GPa. Physics of the Earth and Planetary Interiors, 85, 237–263.

Inoue, T., Yurimoto, H., and Kudoh, Y. (1995) Hydrous modified spinel, Mg$_{1.75}$SiH$_{0.5}$O$_4$: a new water reservoir in the mantle transition region. Geophysical Research Letters, 22, 117–120.

Inoue, T., Tanimoto, Y., Irifune, T., Suzuki, T., Fukui, H., and Ohtaka, O. (2004) Thermal expansion of wadsleyite, hydrous wadsleyite and hydrous ringwoodite. Physics of the Earth and Planetary Interiors, 143–144, 279–290.

Jacobsen, S.D. (2006) Effect of water on the equation of state of nominally anhydrous minerals. In H.J. Keppler and J.R. Smyth, Eds., Water in Nominally Anhydrous Minerals, 62, p. 321–342. Reviews in Mineralogy and Geochemistry, Mineralogical Society of America, Chantilly, Virginia.

Jacobsen, S.D. and Smyth, J.R. (2006) Effect of water on the sound velocities of ringwoodite in the Transition Zone. In S.D. Jacobsen and S. van der Lee, Eds., Earth's Deep Water Cycle, 168, p. 131–145. American Geophysical Union, Geophysical Monograph Series, Washington, D.C.

Jacobsen, S.D., Demouchy, S., Frost, D.J., Boffa-Ballaran, T., and Kung, J. (2005) A systematic study of OH in hydrous wadsleyite from polarized FTIR spectroscopy and single-crystal X-ray diffraction: Oxygen sites for hydrogen storage in the Earth's interior. American Mineralogist, 90, 61–70.

Jeanloz, R. and Hazen, R.M. (1991) Finite strain analysis of relative compressibilities: Application to the high-pressure wadsleyite phase as an illustration. American Mineralogist, 76, 1765–1768.

Jeanloz, R. and Thompson, A.B. (1983) Phase transitions and mantle discontinuities. Reviews in Geophysics and Space Physics, 21, 51–74.

Jung, H. and Karato, S. (2001) Water induced fabric transitions in olivine. Science, 293, 1460–1463.

Kavner, A. (2003) Elasticity and strength of hydrous ringwoodite at high pressure. Earth and Planetary Science Letters, 214, 645–654.

Kiefer, B., Stixrude, L., Hafner, J., and Kresse, G. (2001) Structure and elasticity of wadsleyite at high pressures. American Mineralogist, 86, 1387–1395.

Karato, S. (1990) The role of hydrogen in the electrical conductivity of the upper mantle. Nature, 347, 272–273.

——— (2006) Influence of hydrogen-related defects on the electrical conductivity and plastic deformation of mantle minerals: A Critical Review. In S.D. Jacobsen and S. van der Lee, Eds., Earth's Deep Water Cycle, 168, p. 113–129. American Geophysical Union, Geophysical Monograph Series, Washington, D.C.

Kohn, S.C., Brooker, R.A., Frost, D.J., Slesinger, A.E., and Wood, B.J. (2002) Ordering of hydroxyl defects in hydrous wadsleyite (β-Mg$_2$SiO$_4$). American Mineralogist, 87, 293–301.

Komabayashi, T. (2006) Phase relations of hydrous peridotite: Implications for water circulation in the Earth's mantle. In S.D. Jacobsen and S. van der Lee, Eds., Earth's Deep Water Cycle, 168, p. 29–43. American Geophysical Union, Geophysical Monograph Series, Washington, D.C.

Kudoh, Y. (2001) Structural relation of hydrous ringwoodite to hydrous wadsleyite. Physics and Chemistry of Minerals, 28, 523–530.

Kudoh, Y. and Inoue, T. (1999) Mg-vacant structural modules and dilution of the symmetry of hydrous wadsleyite, β-Mg$_{2-x}$SiH$_{2x}$O4 with 0.00 ≤ x ≤ 0.25. Physics and Chemistry of Minerals, 26, 382–388.

Lager, G.A., Downs, R.T., Origlieri, M., and Garoutte, R. (2002) High-pressure single-crystal X-ray diffraction study of katoite hydrogarnet: Evidence for a phase transition from $Ia3d \rightarrow I4\overline{3}d$ symmetry at 5 GPa. American Mineralogist, 87, 642–647.

Li, B., Liebermann, R.C., and Weidner, D. (1998) Elastic Moduli of Wadsleyite (β-Mg$_2$SiO$_4$) to 7 Gigapascals and 873 Kelvin. Science, 281, 675–677.

Libowitzky, E. and Rossman, G.R. (1997) An IR absorption calibration for water in minerals. American Mineralogist, 82, 1111–1115.

McMillan, P.F., Akaogi, M., Sato, R.K., Poe, B., and Foley, J. (1991) Hydroxyl groups in β-Mg$_2$SiO$_4$. American Mineralogist, 76, 354–360.

Mei, S. and Kohlstedt, D.L. (2000) Influence of water on plastic deformation of olivine aggregates. Journal of Geophysical Research, 105, 21457–21481.

Moore, P.B. and Smith, J.V. (1970) Crystal structure of β-Mg$_2$SiO$_4$: Crystal-chemical and geophysical implications. Physics of the Earth and Planetary Interiors, 3, 166–177.

Mosenfelder, J.L., Deligne, N.I., Asimow, P.D., and Rossman, G.R. (2006) Hydrogen incorporation in olivine from 2–12 GPa. American Mineralogist, 91, 285–294.

O'Neill, B., Bass, J.D., and Rossman, G.R. (1993) Elastic properties of hydrogrossular garnet and implications for water in the upper mantle. Journal of Geophysical Research, 98, B11, 20031–20037.

Ringwood, A.E. (1975) Composition and petrology of the Earth's mantle. McGraw-Hill, New York.

Robinson, K., Gibbs, G.V., and Ribbe, P.H. (1971) Quadratic elongation: a quantitative measure of distortion in coordination polyhedra. Science, 172, 567–570.

Ross, N.L. and Crichton, W.A. (2001) Compression of synthetic hydroxylclinohumite [Mg$_9$Si$_4$O$_{16}$(OH)$_2$] and hydroxylchondrodite [Mg$_5$Si$_2$O$_8$(OH)$_2$]. American Mineralogist, 86, 990–996.

Smyth, J.R. (1987) β-Mg$_2$SiO$_4$; a potential host for water in the mantle? American Mineralogist, 72, 1051–1055.

——— (1994) A crystallographic model for hydrous wadsleyite (β-Mg$_2$SiO$_4$): an ocean in the Earth's interior? American Mineralogist, 79, 1021–1024.

Smyth, J.R. and Frost, D.J. (2002) The Effect of Water on the 410-km Discontinuity: An experimental study. Geophysical Research Letters, 292, 101485, DOI: 10.1029/2001GL014418.

Smyth, J.R. and Jacobsen, S.D. (2006) Nominally anhydrous minerals and the Earth's deep water cycle. In S.D. Jacobsen and S. van der Lee, Eds., Earth's Deep Water Cycle, 168, p. 1–11. American Geophysical Union, Geophysical Monograph Series, Washington, D.C.

Smyth, J.R., Kawamoto, T., Jacobsen, S.D., Swope, R.J., Hervig, R.L., and Holloway, J.R. (1997) Crystal structure of monoclinic hydrous wadsleyite. American Mineralogist, 82, 270–275.

Smyth, J.R., Holl, C.M., Frost, D.J., and Jacobsen, S.D. (2004) High pressure crystal chemistry of hydrous ringwoodite and water in the Earth's interior. Physics of the Earth and Planetary Interiors, 143–144, 271–278.

Smyth, J.R., Frost, D.J., and Nestola, F. (2006) Olivine hydration in the deep upper mantle: Effects of temperature and silica activity. Geophysical Research Letters, 33, L15301.

Tokonami, M. (1965) Atomic scattering factor for O^{2-}. Acta Crystallographica, 19, 486.

van der Lee, S. and Wiens, D.A. (2006) Seismological constraints on Earth's deep water cycle. In S.D. Jacobsen and S. van der Lee, Eds., Earth's Deep Water Cycle, 168, p. 13–27. American Geophysical Union, Geophysical Monograph Series, Washington, D.C.

Wang, Z. and Ji, S. (2001) Elasticity of six polycrystalline silicate garnets at pressure up to 3.0 GPa. American Mineralogist, 86, 1209–1218.

Wood, B.J. (1995) The effect of H$_2$O on the 410-kilometer seismic discontinuity. Science, 268, 74–76.

Young, E.T., Green, H.W., Hofmeister, A.M., and Walker, D. (1993) Infrared spectroscopic investigation of hydroxyl in β-(Mg, Fe)$_2$SiO$_4$ and coexisting olivine: implications for mantle evolution and dynamics. Physics and Chemistry of Minerals, 19, 409–422.

Yusa, H. and Inoue, T. (1997) Compressibility of hydrous wadsleyite (β-phase) in Mg$_2$SiO$_4$ by high pressure X-ray diffraction. Geophysical Research Letters, 24, 1831–1834.

Zha, C-S., Duffy, T.S., Mao, H-K., Downs, R.T., Hemley, R.J., and Weidner, D.J. (1997) Single-crystal elasticity of β-Mg,SiO, to the pressure of the 410 km seismic discontinuity in the Earth's mantle. Earth and Planetary Science Letters, 147, E9–E15.